Qiao *et al. Molecular Cancer* (2024) 23:120
https://doi.org/10.1186/s12943-024-02034-7

Molecular Cancer

RESEARCH Open Access

Diversifying the anthracycline class of anti-cancer drugs identifies aclarubicin for superior survival of acute myeloid leukemia patients

Xiaohang Qiao[1,2*†], Sabina Y. van der Zanden[3†], Xiaoyang Li[4†], Minkang Tan[3], Yunxiang Zhang[4], Ji-Ying Song[6], Merle A. van Gelder[3], Feija L. Hamoen[3], Lennert Janssen[3], Charlotte L. Zuur[1,2], Baoxu Pang[3], Olaf van Tellingen[5], Junmin Li[4,7*] and Jacques Neefjes[3*]

Abstract

The efficacy of anthracycline-based chemotherapeutics, which include doxorubicin and its structural relatives daunorubicin and idarubicin, remains almost unmatched in oncology, despite a side effect profile including cumulative dose-dependent cardiotoxicity, therapy-related malignancies and infertility. Detoxifying anthracyclines while preserving their anti-neoplastic effects is arguably a major unmet need in modern oncology, as cardiovascular complications that limit anti-cancer treatment are a leading cause of morbidity and mortality among the 17 million cancer survivors in the U.S. In this study, we examined different clinically relevant anthracycline drugs for a series of features including mode of action (chromatin and DNA damage), bio-distribution, anti-tumor efficacy and cardiotoxicity in pre-clinical models and patients. The different anthracycline drugs have surprisingly individual efficacy and toxicity profiles. In particular, aclarubicin stands out in pre-clinical models and clinical studies, as it potently kills cancer cells, lacks cardiotoxicity, and can be safely administered even after the maximum cumulative dose of either doxorubicin or idarubicin has been reached. Retrospective analysis of aclarubicin used as second-line treatment for relapsed/refractory AML patients showed survival effects similar to its use in first line, leading to a notable 23% increase in 5-year overall survival compared to other intensive chemotherapies. Considering individual anthracyclines as distinct entities unveils new treatment options, such as the identification of aclarubicin, which significantly improves the survival outcomes of AML patients while mitigating the treatment-limiting side-effects. Building upon these findings, an international multicenter Phase III prospective study is prepared, to integrate aclarubicin into the treatment of relapsed/refractory AML patients.

†Xiaohang Qiao, Sabina Y. van der Zanden and Xiaoyang Li contributed equally to this work.

*Correspondence:
Xiaohang Qiao
x.qiao@nki.nl
Junmin Li
drlijunmin@126.com
Jacques Neefjes
j.j.c.neefjes@lumc.nl

Full list of author information is available at the end of the article

Graphical abstract

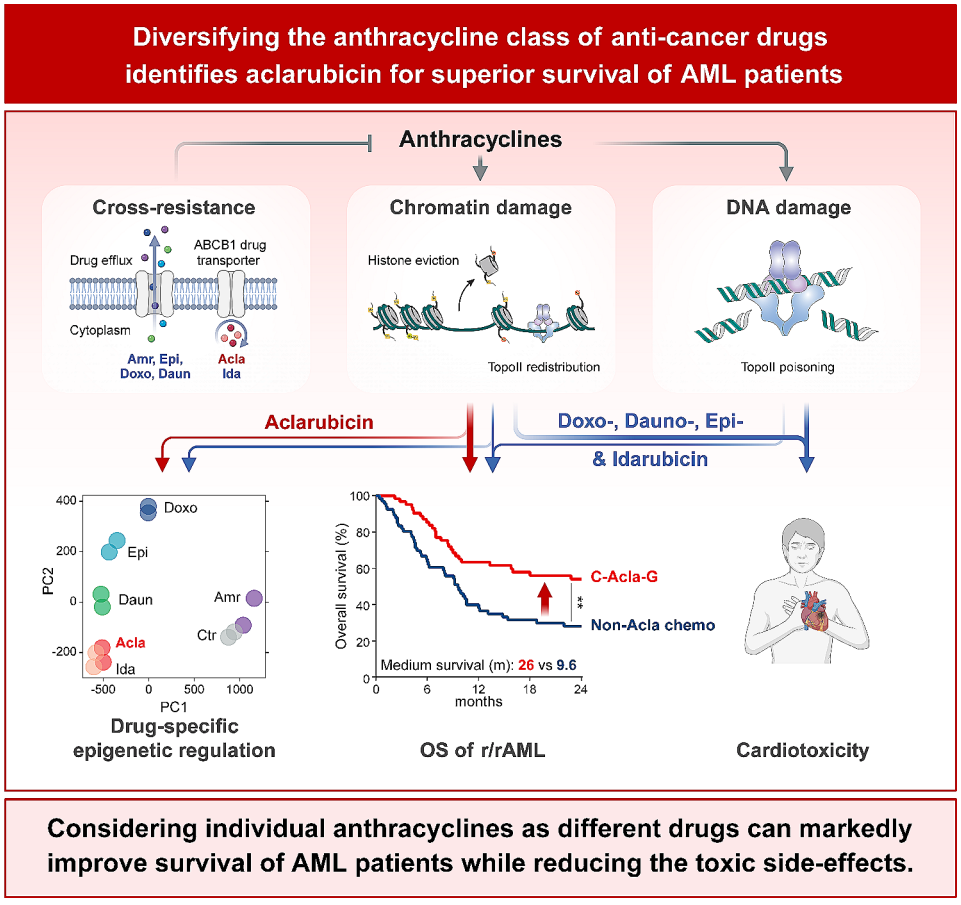

Keywords Anthracycline, Doxorubicin, Aclarubicin, Refractory/relapsed acute myeloid leukemia, Cardiotoxicity, Histone eviction, Chromatin damage, DNA damage, Bio-distribution, Cross-resistance

Background

Most anthracyclines function as poisons of the enzyme topoisomerase II (TopoII) that trap it on chromatin in a state inducing DNA breaks [1]. In addition, these drugs also evict histones from defined genomic areas, leading to delay of DNA damage repair and alterations in epigenome and transcriptome, collectively termed chromatin damage [2–4]. Histone eviction emerges as a major cytotoxic mechanism of anthracyclines [5]. TopoII poisons, like etoposide, which solely induce DNA damage are considerably less effective in cancer treatment [2, 6], and also less toxic [5, 7]. On the contrary, aclarubicin that only induces histone eviction without causing DNA damage is highly effective in treating *de novo* acute myeloid leukemia (AML) [5, 8]. Hence, DNA damage appears not to be a prerequisite for effective anticancer activities of anthracycline drugs. We previously reported that the combination of DNA-damaging and chromatin-damaging activities leads to the cardiotoxicity and therapy-related tumorigenesis of anthracyclines [5]. Selectively eliminating the DNA-damaging activity of anthracycline from its chromatin-damaging activity through chemical modification mitigates these devastating side effects, without hampering their anti-cancer efficacies [5]. Cancer patients receiving anthracycline chemotherapy have more than twice the risk of developing heart failure compared to their peers without cancer [9, 10]. Moreover, this risk continues to increase with the survival time of cancer survivors [10]. Exceeding the recommended cumulative dose precipitates a sharp rise in cardiotoxicity [11]. Therefore, the cardiotoxicity of anthracyclines significantly limits patients from extending treatment and affects their quality of life. Clinical application of low cardiotoxic anthracyclines will confer major benefits in cancer therapy, expanding treatment options for patients with comorbidities including older adults [12] and reducing late effects, particularly for pediatric patients [13]. Low cardiotoxic anthracyclines would

allow long-term treatment, while the current cardiotoxic anthracyclines limit treatment due to cumulative dose-dependent cardiotoxicity.

Here, we systematically evaluated anthracycline drugs currently used in clinic against a series of key features to determine whether they differ in terms of anti-neoplastic potency, site of action and toxicity profiles. We identified aclarubicin, an anthracycline currently used only in Asia for AML patients with high comorbidity indices, as a promising variant devoid of cardiotoxicity. Notably, aclarubicin can be safely administered even after maximum exposure to doxorubicin or idarubicin in mice and humans. When used in second line, aclarubicin-based regimen significantly increases the overall survival of relapsed/refractory AML patients by 23% compared to other intensive chemotherapy approaches. These findings illustrate how aclarubicin can improve the treatment of relapsed/refractory AML patients that currently have a poor prognosis, addressing a major unmet need in current oncology practice.

Methods

Reagents

Doxorubicin and etoposide were purchased from Pharmachemie (The Netherlands), daunorubicin was obtained from Sanofi-Aventis and epirubicin was obtained from Accord Healthcare Limited (UK), idarubicin was obtained from Pfizer and Santa Cruz Biotechnology (sc-204774). Aclarubicin for in vivo mouse experiments was obtained from Shenzhen Main Luck Pharmaceuticals Inc. Aclarubicin (for in vitro experiments, sc-200160) and amrubicin (sc-207289) were obtained from Santa Cruz Biotechnology.

Cell culture

K562 (B. Pang, LUMC Leiden, The Netherlands, RRID: CVCL_K562), MM6 (RRID: CVCL_1426), MOLM13 (RRID: CVCL_1426), MV4:11 (RRID: CVCL_0064), U937 (RRID: CVCL_0007) (all four lines were a gift from L. Smit, VUMC Amsterdam, The Netherlands) and THP-1 (ATCC, Manassas, VA, RRID: CVCL_0006) were cultured in RPMI-1640 medium supplemented with 8% fetal calf serum (FCS, SERANA, S-FBS-CO-015). OCI-AML-2 (DSMZ, ACC-No 99, RRID: CVCL_1619) and OCI-AML-3 (DSMZ, ACC-No 582, RRID: CVCL_1844) (M. Griffioen, LUMC Leiden, The Netherlands) and OCI-AML-4 (M.L.M. Jongsma, LUMC Leiden, The Netherlands, RRID: CVCL_5224) were cultured in IMDM medium supplemented with 8% FCS and glutamine. MelJuSo (RRID: CVCL_1403) cells were maintained in IMDM supplemented with 8% FCS. All cell lines were maintained in a humidified atmosphere of 5% CO_2 at 37 °C, regularly tested for the absence of mycoplasma and STR profile.

Cell line construction

For endogenous tagged GFP-H2B K562 cells, mScarlet was swapped for GFP in the homology repair construct using NheI and BglII and cells were generated as described [5]. Co-transfection into K562 cells was done by electroporation using Lonza SF cell line kit. ABCB1 overexpressing K562 cells were generated as described [14]. Endogenous tagged 3×Flag-TopoIIα K562 cell line was generated using HR-3×Flag construct designed at least 40 base pairs up- and downstream of the genomic TopoIIα stop codon. The gRNA target sequence was designed using the Zhang Lab CRISPR tool (http://crispr.mit.edu/) and cloned into the pX330 vector (RRID: Addgene_110403). Primers used for the HR construct: 5'-CACCGATGATCTGTTTTAAAATGTG-3' and 5'-AAACCACATTTTAAAACAGATCATC-3'. Co-transfection of ssDNA oligo and CRISPR plasmid (pX459) into K562 cells was performed by electroporation using Lonza SF cell line kit. Primers used for genotyping were forward primer: 5'-TAAGCAGAATTCATGCCACTTATTTGGGCAAT-3' and reverse primer: 5'-TGCTTAAAGCTTTGCCCATGAGATGGTCACTA-3'.

DNA damage assessed by Western blot and constant field gel electrophoresis

After 2-hour drug treatment of indicated drugs at 5 μM, THP-1 cells were washed with PBS, and then lysed directly in sodium dodecyl sulfate (SDS)-sample buffer (2% SDS, 10% glycerol, 5% β-mercaptoethanol, 60 mM Tris-HCl pH 6.8, and 0.01% bromophenol blue). Lysates were resolved by SDS/polyacrylamide gel electrophoresis followed by Western blotting. Primary antibodies used for blotting were γH2AX (1:1,000, 05-036, Millipore) and β-actin (1:10,000, A5441, Sigma, RRID: AB_476744). CFGE were performed as described [15]. Images were quantified with ImageJ (RRID: SCR_003070).

Fractionation assay

Endogenously tagged GFP-H2B K562 cells (1×10^6) were pre-incubated with protease inhibitor cocktail (P1860-1ML, Sigma-Aldrich) for 1 h followed by 3-hour treatment with 10 μM of the indicated drugs. Cells were dissolved in lysis buffer (50 mM Tris-HCl pH 8.0, 150 mM NaCl, 5 mM $MgCl_2$, 0.5% NP40, 2.5% glycerol supplemented with protease inhibitors and 10 mM NMM) for 5 min on ice, and then centrifuged for 10 min at 15,000 g at 4 °C. Both nucleus (pellet) and cytosol (supernatant) were washed once and then submitted for Western Blot analysis. Primary antibodies used for detection: GFP (1:1,000) [16], Lamin B1 (1:1,000, 12,987-I-AP, Proteintech, RRID: AB_2136290), and Calnexin (1:1,000, #2679, Cell Signaling Technology, RRID: AB_2228381).

Time-lapse confocal microscopy

For time-lapse confocal imaging, MelJuSo cells were seeded in 35-mm glass bottom petri dish (Poly-D-Lysine coated, MatTek Corporation), transfected with TopoIIα-GFP construct using Effectene (301425, QIAGEN) and imaged upon treatment with the indicated drugs [2]. Leica SP8 confocal microscope system, 63× lens, equipped with a climate chamber was used. TopoIIα-GFP distribution was quantified using Leica Application Suite X software (RRID: SCR_013673).

Short-term cell viability assay

Twenty-four hours after seeding into 96-well plates, cells were treated with indicated drugs for 2 h at physiologically relevant concentrations [2]. Subsequently, drugs were removed by extensive washing, and cells were cultured for an additional 72 h, according to their pharmacokinetics. Cell viability was measured using the CellTiter-Blue viability assay (G8080, Promega). Survival was normalized to the untreated control samples after correction for the background signal.

ChIP-seq

Endogenous tagged 3×Flag-TopoIIα K562 cells were treated with 10 μM of indicated drugs for 4 h. Cells were fixed and processed as described [3, 17]. ChIP was done with anti-Flag M2 antibody (F3165, Sigma, RRID: AB_259529), followed by sequencing on an Illumina Hiseq2000 platform (Genome Sequencing Service Center of Stanford Center for Genomics and Personalized Medicine Sequencing Center).

ChIP-seq data were processed identically using the ENCODE Data Coordination Center (DCC) ChIP-seq pipeline (https://github.com/ENCODE-DCC/chip-seq-pipeline2) (v1.9.0). Briefly, the ChIP-seq reads were aligned to the human reference genome (GRCh37/hg19) using Bowtie2 (RRID: SCR_016368) [18]. Duplicate reads were removed using Picard MarkDuplicates (RRID: SCR_006525). Peaks of each sample were called against the whole-cell lysate replicates using SPP (RRID: SCR_001790) [19] with the parameters '-npeak 300000 -speak 155 -fdr 0.01'. The blacklisted regions described by ENCODE were discarded [20]. Reproducible peaks were intersected from two biological replicates and annotated with epigenomic signatures of K562 cells, downloaded from the Roadmap Epigenomics Project (RRID: SCR_008924) [21]. Normalized TopoIIα binding affinity matrix: consensus peaks by samples, principle component analysis and differential binding affinity analysis were performed using the R package DiffBind (RRID: SCR_012918) [22].

ATAC-seq

Wild-type K562 cells were treated with 10 μM of indicated drugs for 4 h. Cells were fixed and processed as described [23, 24]. DNA was processed using a customized library preparation method for ATAC-seq and was sequenced using an Illumina HiSeq4000 platform.

ATAC-seq data were processed identically using the ENCODE Data Coordination Center (DCC) ATAC-seq pipeline (https://github.com/ENCODE-DCC/atac-seq-pipeline) (v1.10.0). Briefly, the ATAC-seq reads were aligned to the human reference genome (GRCh37/hg19) using Bowtie2 [18]. Duplicate reads were removed using Picard MarkDuplicates (RRID: SCR_006525). Peaks were called using MACS2 (RRID: SCR_013291) [25] with the setting of '-p 0.01 --shift −75 --extsize 150 --nomodel -B --SPMR --keep-dup all', then followed by blacklisted regions filtering described by ENCODE [20]. Reproducible peaks were identified from two biological replicates and annotated with epigenomic signatures of K562, downloaded from the Roadmap Epigenomics Project [21]. ATAC-seq signal tracks for all the samples were generated by BEDTools (RRID: SCR_006646) with the command 'bedtools genomecov -scale' using the read count per million (CPM) normalization and convert to bigwig files using bedGraphToBigWig. Normalized ATAC-seq read density matrix: consensus peaks by samples, principle component analysis and differential chromatin accessibility analysis were performed using the R package DiffBind [22].

Principal component analysis (PCA)

The reproducible peaks were identified by intersecting two biological replicates of each drug treatment, and then merged into consensus peak set. Subsequently, the read density was quantified for the consensus peaks to create an input matrix for PCA analysis. The dba.plotPCA function of DiffBind package was applied to calculate the principal components through eigenvector decomposition of the covariance matrix from the input matrix. The maximum variance of projected data by principal component 1 and 2 were plotted in the x- and y-axis accordingly.

DNA dye exclusion assay

Circular DNA (1 μg/ml) was incubated with Quant-iT PicoGreen dsDNA reagent (P7581, Thermo Fisher Scientific) for 5 min at room temperature (RT). Subsequently, drug was added to the DNA/PicoGreen mix at indicated concentrations and incubated for another 5 min at RT. Following the reaction, the PicoGreen fluorescence was measured using CLARIOstar plate reader (BMG labtech) with excitation at 480 nm and emission at 520 nm (48020/52010 filter). The fluorescence was quantified relative to untreated controls. Fluorescent signals of all

samples were corrected for the corresponding drug concentrations in the absence of DNA.

Bio-distribution of anthracyclines in mice

FVB/NRj mice (RRID: MGI:6364162) ordered from Janvier Labs (Le Genest-Saint-Isle, France) were housed in individually ventilated cages under specific pathogen-free conditions in the animal facility of the NKI (Amsterdam, The Netherlands). All mouse experiments were approved by the Animal Ethics Committee of the NKI and were performed according to institutional and national guidelines. Male mice (8-week old) were i.v. injected with doxorubicin, aclarubicin, amrubicin, epirubicin or idarubicin at 5 mg/kg ($n=5$ per group). Four hours post injection, animals were sacrificed, and plasma, heart, lung, liver, kidney, spleen, brain, thymus, axillary+inguinal lymph nodes, and testis+epididymis were collected. Hearts were cut into two pieces with coronal section. One piece was fixed in EAF fixative (ethanol/acetic acid/formaldehyde/saline, 40:5:10:45 v/v/v/v) and processed for Phospho-H2AX (Ser139) IHC (1:100, #2577, Cell Signaling Technology). The other half of the heart and the rest of organs were weighed and frozen.

Calibration samples for each anthracycline with defined concentration were prepared in blank tissue homogenates. Daunorubicin was used as internal standards. Of each sample, a 100 µl tissue homogenate was mixed with 200 µl of 0.1% formic acid, 1 ml of Chloroform:2-propanol (1:1) and 10 µl of internal standard, then vortexed vigorously for 5 min, followed by centrifugation at 5,000 g for 5 min at 4 °C. The aqueous layer and the intermediate layer were removed by suction. The organic layer was decanted into a clean polypropylene tube and evaporated by Savant Speed-Vac SC210A concentrator (Thermo Fisher Scientific, Waltham, USA) at 35 °C. The residue was reconstituted in 150 µl of DMSO, vortexed for 20 sec and then sonicated for 5 min. After centrifuged at >12,000 g for 2 min, 10 µl of supernatant was analyzed by liquid chromatography-tandem mass spectrometry (LC-MS)/MS, which consisted of an API 3500 mass spectrometer (Sciex, Framingham, MA) coupled to an UltiMate 3000 LC System (Dionex, Sunnyvale, CA). Samples were separated using a ZORBAX Extend-C18 column (Agilent, Santa Clara, CA), kept at 50 °C preceded by a Securityguard C18 pre-column (Phenomenex, Utrecht, The Netherlands). Elution was done using a mixture of mobile phase A (0.1% formic acid in water (v/v)) and mobile phase B (methanol) in a 2 min gradient from 20 to 95% B, followed by 95% B that was maintained for 3 min and then re-equilibrated at 20% B. Multiple reaction monitoring parameters were 544.0/397.0 (doxorubicin and epirubicin), 498.1/291 (idarubicin), 812.4/570.3 (aclarubicin), 484.2/333.1 (amrubicin) and 528.1/321.1 (daunorubicin). System control and data analysis were done using Analyst® 1.6.2 software (AB Sciex; Foster City, CA).

The cardiotoxicity of anthracyclines in mice

FVB/NRj mice (10–11-week old, RRID: MGI:6364162) were i.v. injected with 5 mg/kg of doxorubicin, 5 mg/kg of aclarubicin, or 5 ml/kg of saline every 2 weeks for 4 times. After 4-week interval, the animals were i.v. injected with 5 mg/kg of indicated drug or 5 ml/kg of saline every 2 weeks for another 4 times. The mice were monitored every other day. When body weight loss was more than 20%, or circulation failure occurred, animals were euthanized by CO_2. Subsequently, full body anatomy was performed. All organs were collected, fixed in EAF fixative and embedded in paraffin. Sections were cut at 2 µm from the paraffin blocks and stained with hematoxylin and eosin, and 4 µm for immunohistochemistry of Desmin (1:200, M0760, DakoCytomation), Vimentin (1:100, #5741, Cell Signaling Technology, RRID: AB_10695459), or Periostin (1:100, ab215199, Abcam, RRID: AB_2924310). Pathology slides were reviewed twice by an expert mouse pathologist who was blind to the treatment. Incidence rate (IR = [number of mice with the specific side effect over a time period]/[sum of mice × time at risk during the same time period]) and cumulative incidence (CI = [number of mice with specific side effect at end time point]/[total number of mice at start]) were calculated for cardiotoxicity.

AML patient data analyses

Patients with refractory or relapsed AML treated between July 2012 and July 2022 at Ruijin hospital, China were enrolled in this retrospective study. Some patients participated in trial ChiCTR-OPC-14,005,712, ChiCTR-OPC-15,006,896, ChiCTR-IIR-16,008,809, ChiCTR-OIC-16,008,952, ChiCTR-IIR-16,008,962 and ChiCTR-IIR-17,011,677. This study was approved by the ethics committee of Ruijin Hospital, all patients provided written informed consent.

Cytogenetic risk was classified according to the modified Southwest Oncology Group criteria [26]: (1) favorable risk, including t(8;21) and inv(16) or t(16;16) (p13;q22); (2) unfavorable risk, including del(5q) or monosomy 5, monosomy 7 or del(7q), abnormal 3q, 9q, 11q, 21q, or 17p, t(6;9), t(9;22), and complex karyotypes (three or more unrelated chromosomes abnormal); and (3) intermediate risk, including normal karyotypes and all other anomalies. FLT3 internal tandem duplication (FLT3-ITD) and mutations in CEBPA, NPM1 and IDH1/2 were tested. Integrated risk was classified as described [27]. Complete remission was defined as bone marrow blasts < 5%, absolute neutrophil count $\geq 1\times10^9$/L, and platelet count $\geq 100\times10^9$/L, and absence of extramedullary disease. Partial remission was defined as

having < 15% (and a 50% decrease in bone marrow blasts) but > 5% blasts or with < 5% blasts but not reaching the CR criteria for blood cell count or clinical manifestation. The baseline characteristics and clinical outcomes of the patients are summarized in supplemental Tables S1 and S2, respectively.

AML treatments

CAG patients were treated with 15–25 mg/m^2 of cytarabine (Ara-C) injected s.c. every 12 h on days 1–14, 20 mg/day of aclarubicin infused i.v. on days 1–4, and 200 μg/m^2 of granulocyte stimulating factor (G-CSF) administered s.c. daily on days 1–14. G-CSF was reduced, or temporarily stopped when neutrophilia was > 5×10^9/L. IA patients were treated with 6–10 mg/m^2 of idarubicin infused i.v. on days 1–3 and 100–200 mg/m^2 of Ara-C on days 1–7. VA patients were injected with 75 mg/m^2 of azacitidine s.c. daily on days 1–7, and administered with venetoclax orally, once daily. The dose of venetoclax was 100 mg on day 1 and 200 mg on day 2; and 400 mg on days 3–28. In all subsequent 28-day cycles, the dose of venetoclax was initiated at 400 mg daily. The other induction chemotherapies for r/rAML patients included IA, DA, FLAG, CLAAG and CHA regimens. For patients treated with DA regimen, 20 mg/m^2 of decitabine was administered i.v. daily on days 1–5, and 1 g/m^2 of Ara-C was injected every 12 h on days 6–7. For patients treated with FLAG regimen, fludarabine was infused i.v. at 30 mg/m^2 on days 2–6; 4 h after fludarabine infusion, Ara-C was injected i.v. at 1.5–2 g/m^2 over 3 h on days 2–6; G-CSF was administered at 5 μg/kg s.c. on days 1–5; additional G-CSF may be administered since 7 days after the end of chemotherapy until white blood cell count > 500/μL. For patients > 60-year-old, the dose may be reduced to 20 mg/m^2 for fludarabine and 0.5–1 g/m^2 for cytarabine. For patients treated with CLAAG regimen, 5 mg/m^2 of cladribine was infused i.v. over 2 hours on days 1–5; 15 mg/m^2 of Ara-C was injected s.c. every 12 h on days 1–10; trans retinoic acid (ATRA) was administered orally at 45 mg/m^2 on days 4–6, then at 15 mg/m^2 on days 7–20; 300 μg G-CSF was injected s.c. on day 0. For patients treated with CHA regimen, 5 mg/m^2 of cladribine was infused i.v. over 2 hours on days 1–5; 2 mg/m^2 of homoharringtonine was infused i.v. over 2 hours on days 1–5; 1 g/m^2 of Ara-C was injected 2 hours after cladribine on days 1–5.

Statistical analyses

Results are shown as mean ± SEM or mean ± SD. Statistical analysis was performed using GraphPad Prism (RRID: SCR_002798) unless otherwise specified. All in vitro experiments were performed with a minimum of three independent trials with the exception of ChIP-seq and ATAC-seq which were biological duplicates. All individual animals in mouse experiments are shown in the dot plots. Statistical tests are indicated in each figure legend. Survival curves were analyzed by the log-rank (Mantel-Cox) test. Statistical analysis of pathology quantification was determined using the Student's *t*-test or Mann-Whitney test. Kinetic analysis was performed with Two-way ANOVA. Clinical outcomes were analyzed by Fisher's exact test or Mantel-Haenszel test. *P* values of < 0.05 were considered statistically significant.

Results

Mechanisms of action and cross-resistance of anthracyclines

To assess whether the clinically administered anthracyclines (Fig. 1A) differ in their DNA- and chromatin-damaging activities, as well as cross-resistance, we exposed an AML cell line THP-1 to clinically relevant doses for 2 h [28]. DNA damage was evaluated using constant-field gel electrophoresis (CFGE) [15] and detection of phosphorylation of H2AX at Ser139 (γH2AX) [29] by Western blotting. The anthracyclines, doxorubicin (Doxo), daunorubicin (Daun), epirubicin (Epi), idarubicin (Ida), amrubicin (Amr) and structure-unrelated TopoII poison etoposide (Etop) all induced DSBs, unlike aclarubicin (Acla) (Fig. 1B–E). Next, chromatin damage as the result of histone eviction was visualized using fractionation assay in K562 cells with endogenously tagged GFP-H2B. Except for Amr, all the tested anthracyclines induced histone release from nucleus and accumulation in cytosol (Fig. 1F, G; Fig. S1A). Furthermore, histone-evicting anthracyclines also redistributed GFP-TopoIIα on chromatin (Fig. S1B, C). Cytotoxicity assays revealed poor anti-cancer activity for the DNA-damaging analog Amr, while the other analogs bearing chromatin-damaging activity were effective in eliminating various myeloid leukemia cell lines (Fig. 1H).

In addition to treatment-limiting cardiotoxicity, drug resistance could also limit the effect of anthracycline drugs. ABCB1, a major drug efflux transporter, contributes to anthracycline resistance [30, 31]. We generated a Doxo-resistant leukemia cell line by overexpressing ABCB1 [14] and tested its sensitivity to other anthracyclines (Fig. 1I–K; Fig. S1D). The ABCB1-overexpressing cells acquired resistance to Doxo, Daun, Epi and Amr, but failed to export Ida and Acla efficiently (Fig. 1J, K). These findings suggest that clinically relevant anthracyclines should be considered as distinct drugs with unique features and varying efficiencies. Evicting histones and relocalizing TopoIIα while not inducing detectable DNA damage, as in the case of Acla, appears adequate for efficient cytotoxicity.

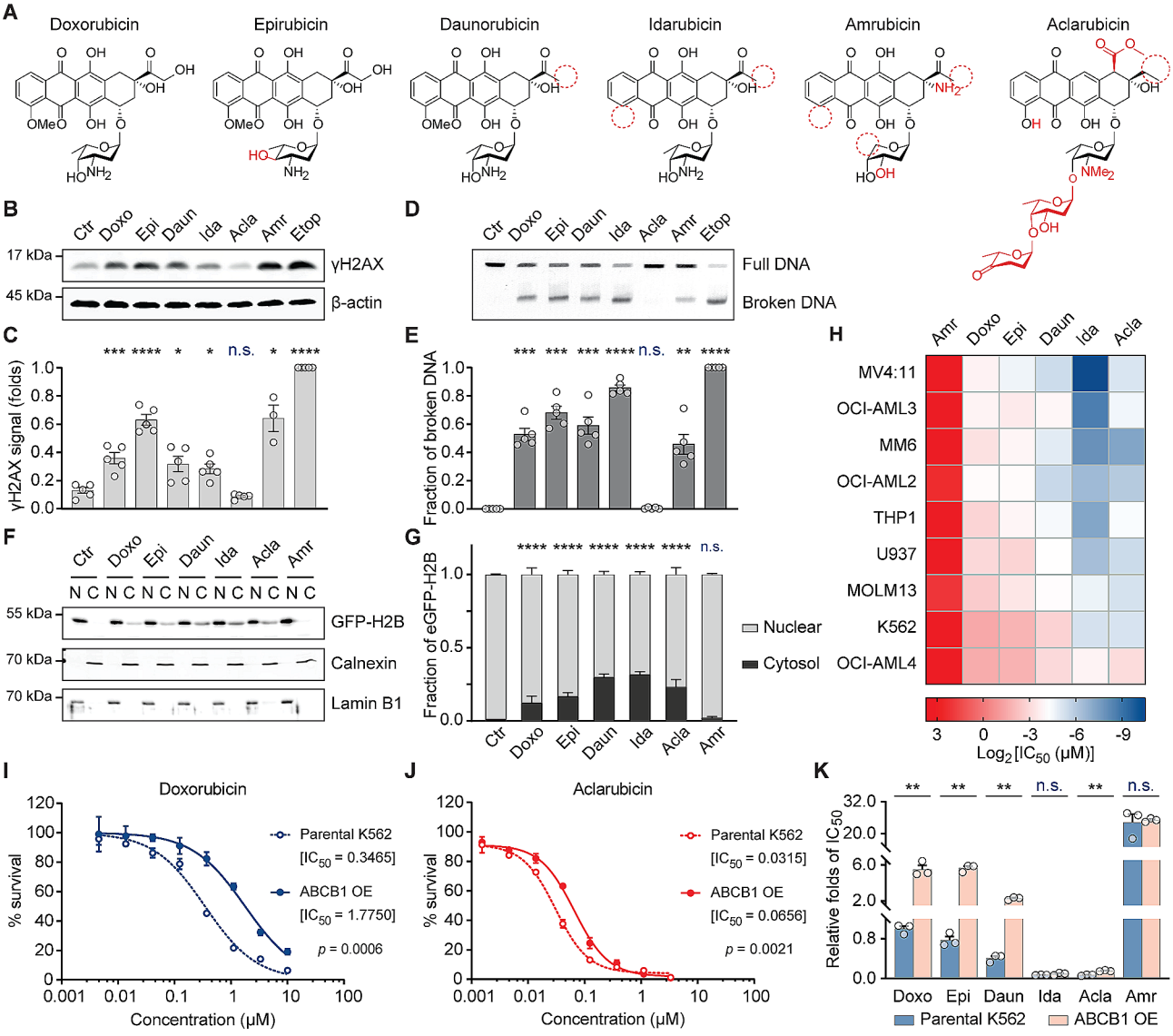

Fig. 1 Acla differs from other anthracyclines in mechanisms of action and cross-resistance. (**A**) Structures of anthracyclines used in this study. Chemical features divergent from Doxo are depicted in red. (**B**) DNA damage examined by γH2AX Western blot in THP-1 cells. (**C**) Quantification of the γH2AX signal normalized to β-actin. Data are mean ± SEM; $n = 4$ biological replicates; Student's *t*-test. (D) DSBs analyzed by CFGE in THP-1 cells. (**E**) Quantification of relative broken DNA in (**D**). Data are mean ± SEM; $n = 4$ biological replicates; Student's *t*-test. (**F**) Histone eviction revealed by cell fractionation assay in K562-eGFP-H2B cells. N, nuclear fraction; C, cytosolic fraction. Calnexin and Lamin B1 are the loading control of each fraction. (**G**) The distribution of eGFP-H2B was quantified for both compartments. Data are mean ± SD; $n = 4$ biological replicates; two-way ANOVA. (**H**) IC_{50} of each anthracycline in different leukemia cell lines. (**I, J**) Cell viability of parental K562 cells and ABCB1-overexpressing K562 cells upon Doxo (**I**) and Acla (**J**) treatment. Data are mean ± SD; $n = 3$ biological replicates; two-way ANOVA. (**K**) Relative IC_{50} folds of each condition compared to that of Doxo in parental K562 cells. Data are mean ± SEM; $n = 3$ biological replicates; Student's *t*-test. *$P < 0.05$, **$P < 0.01$, ***$P < 0.001$, and ****$P < 0.0001$; n.s., not significant

Epigenetic selectivity of TopoIIα redistribution and histone eviction of anthracyclines

Anthracyclines poison TopoII by disrupting its interface with DNA and trapping TopoII prior or after DNA damage formation. The cyclohexene ring ensures DNA intercalation while the sugar moiety fills the minor groove and attacks TopoII [32]. However, the anthracycline-specific redistribution of TopoII and its association with histone eviction have not been characterized. We addressed this in K562 cells, whose epigenomic landscape has been extensively profiled by the ENCODE consortium [33]. Chromatin immunoprecipitation followed by deep sequencing (ChIP-seq) against endogenously tagged TopoIIα was performed 4 h post anthracycline exposure in two independent experiments (Fig. S2A). Although anthracyclines can be sufficiently washed out from samples, trace amount of drugs might remain DNA-bound due to their intercalating properties [34]. The distribution

pattern of total reads for anthracyclines did not align with that of DNA intercalating activity, suggesting that any residual anthracycline in the DNA did not significantly interfere with the subsequent sequencing steps (Supplementary Excel file; Fig. S2B).

Principal component analysis (PCA) of the resulting ChIP-seq profiles suggested that all histone-evicting anthracyclines cause extensive and drug-specific TopoIIα redistribution compared to untreated or Amr-treated cells (Fig. 2A, B). To characterize this drug-specific TopoIIα redistribution, we integrated the ChIP-seq data

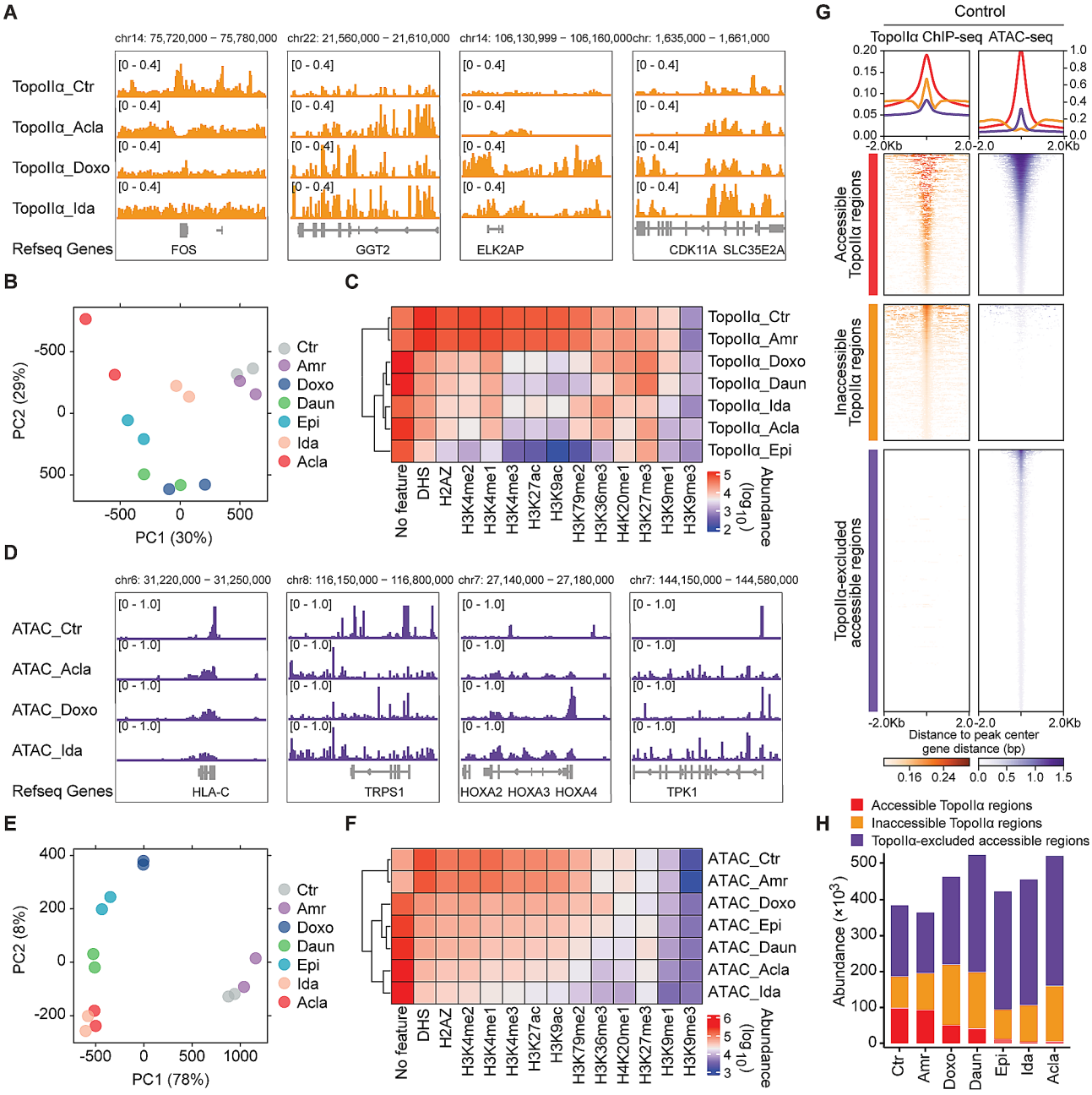

Fig. 2 Epigenetic selectivity of TopoIIα redistribution and histone eviction of anthracyclines. (**A**) Illustration of drug-specific TopoIIα redistribution revealed by ChIP-seq. (**B**) Principal component analysis (PCA) of TopoIIα ChIP-seq data. Two independent biological replicates were included for each condition. (**C**) Heatmap of TopoIIα peak abundance associated with specific histone features derived from Roadmap Epigenomics Project. (**D**) Illustration of drug-specific accessible chromatin regions revealed by ATAC-seq. (**E**) PCA analysis of ATAC-seq data. Two independent biological replicates were included for each condition. (**F**) Heatmap of ATAC peak abundance associated with specific histone. (**G**) Density plots showing the accessible and inaccessible TopoIIα regions, and TopoIIα-excluded accessible regions surrounding ± 2 kb from the center of the detected peaks in the untreated K562 cells. (**H**) The abundance of each category in different conditions

with the epigenetic information from ENCODE (Fig. 2C). Anthracyclines with the similar sugar moiety and cyclohexane (Fig. 1A), such as Daun and Doxo (also named as hydroxyDaun), depleted TopoIIα from active chromatin regions, including DNase I hypersensitive regions (DHS), H3K4me1-, H3K4me2-, H3K4me3-, H3K9ac-, H3K27ac-, H3K79me2- and H2A.Z-associated regions [35]. Instead, TopoIIα was trapped in compact chromatin regions marked by H3K27me3 [35], H3K9me1 [36] and H3K9me3 [37] (Fig. 2C). Ida and Acla depleted TopoIIα from broader chromatin states, except for H3K9me3- [37], H3K27me3- [35] and H3K36me3-decorated regions [37] (Fig. 2C). Epi, with an epimerizing hydroxyl group at the sugar moiety (Fig. 1A), further depleted TopoIIα from H3K36me3-modified regions [37] (Fig. 2C). It is worth noting that the redistribution of TopoIIα at regions with unknown epigenetic features was increased for all drugs, except for Amr (Fig. 2C).

While the TopoIIα redistribution exhibited drug specificity, we further investigated the histone eviction preferences of each anthracycline using transposase-accessible chromatin with sequencing (ATAC-seq) [23] in wild-type K562 cells (Fig. 2D). In line with its lack of chromatin-damaging activity (Fig. 1F, G), Amr failed to induce *de novo* open chromatin and clustered closely with untreated cells in PCA plot (Fig. 2E). Similar to the pattern of TopoIIα redistribution, the other tested anthracyclines predominantly evicted histones from open chromatin regions, highlighting their distinct preferences (Fig. 2F). The integration of TopoIIα ChIP-seq and ATAC-seq revealed a connection between histone eviction and TopoIIα depletion in transcriptionally active regions, suggesting that selective histone eviction may contribute to the observed depletion of TopoIIα in these regions (Fig. 2G, H; Fig. S2C). However, the presence of a significant number of non-overlapping regions between TopoIIα redistribution and *de novo* accessible chromatin suggests that they may constitute two independent effects of anthracyclines (Fig. S2C). The individual genomic preferences of clinically used anthracyclines imply that they should be considered as distinct drugs.

Bio-distribution of anthracyclines

Acla is effective in eliminating a large variety of cancer cells in tissue culture [5]. However, its clinical use is primarily confined to AML treatment, showing less efficacy against solid tumors [38, 39]. This discrepancy may stem from differences in biodistribution of anthracyclines. To test this, we performed a comprehensive bio-distribution study comparing Acla with the other clinically used anthracyclines in mice. Four hours post i.v. injection of a clinically relevant dose (5 mg/kg) [40] of indicated drug, Doxo, Epi and Ida exhibited similar bio-distribution patterns across different organs (Fig. 3A; Fig. S3A). Although Amr had a similar tissue distribution as Doxo, it showed reduced accumulation in lungs, kidneys, and heart. A notable exception was Acla, which accumulated in lymphoid organs (spleen, thymus and lymph nodes) but poorly distributed to other tissues (Fig. 3A; Fig. S3A). Acla rapidly decreased in plasma (Fig. 3A; Fig. S3A), mirroring observations in humans, mainly due to metabolism [41]. This distinct distribution pattern may explain the limited efficacy of Acla in treating solid tumors, as opposed to hematologic tumors. Brain tissue was poorly penetrated by all drugs (Fig. 3A; Fig. S3A).

Furthermore, we evaluated DNA damage in the heart following drug exposure. While Doxo, Epi and Ida induced persistent DNA damage in the heart, the hearts of Acla- and Amr-treated mice did not show any γH2AX signals 4 h post drug administration (Fig. 3B; Fig. S3B). This observation aligns with the poor tissue penetration of Acla and Amr, and the fact that Acla does not induce detectable DNA damage.

Acla is safe and well tolerated following Doxo treatment

Anthracyclines like Doxo, Daun, Ida and Epi are known to induce cumulative dose-dependent cardiotoxicity, often restricting patient treatment to a limited number of courses. Given that Acla treatment does not entail cardiotoxicity risk [5], we reasoned that it might be safe to administer this drug to mice following the treatment of cardiotoxic anthracyclines. To test this, mice received Acla injection after half-maximum cumulative dose of Doxo (Fig. 4A) and were monitored over time.

Doxo-induced cardiotoxicity resulted in cardiac hypertrophy and remodeling, evident from thrombus formation in the left atrium and auricle, accompanied by inflammation, fibrosis and calcification [5, 42] (Fig. 4B; Fig. S4A). Further staining for profibrotic proteins vimentin [43] and periostin [44], and cytoskeletal protein desmin [45], revealed myocyte impairment and stromal fibrosis (Fig. 4C–H; Fig. S4B–F). Ultimately, Doxo-treated mice died from circulation failure due to impaired cardiac function (Fig. 4I).

Consistent with clinical observations [9] and our previous findings [5], the incidence, latency and histopathological alterations of Doxo-induced cardiotoxicity manifested in a dose-dependent manner (Fig. 4, D-C vs. D-D). In contrast, eight courses of Acla treatment did not elicit any abnormalities in the heart (Fig. 4F–K; Fig. S4, A-A vs. C-C/D-C/D-D). More importantly, Acla treatment after half-maximum cumulative dose of Doxo did not aggravate cardiotoxicity (Fig. 4; Fig. S4, D-A vs. D-D). Likewise, pre-treatment of Acla did not render mice more susceptible to Doxo-induced cardiotoxicity (Fig. 4; Fig. S4, A-D vs. D-C/D-D). Hence, Acla is safe and well tolerated following Doxo treatment in this model system. Considering its limited cardiotoxicity,

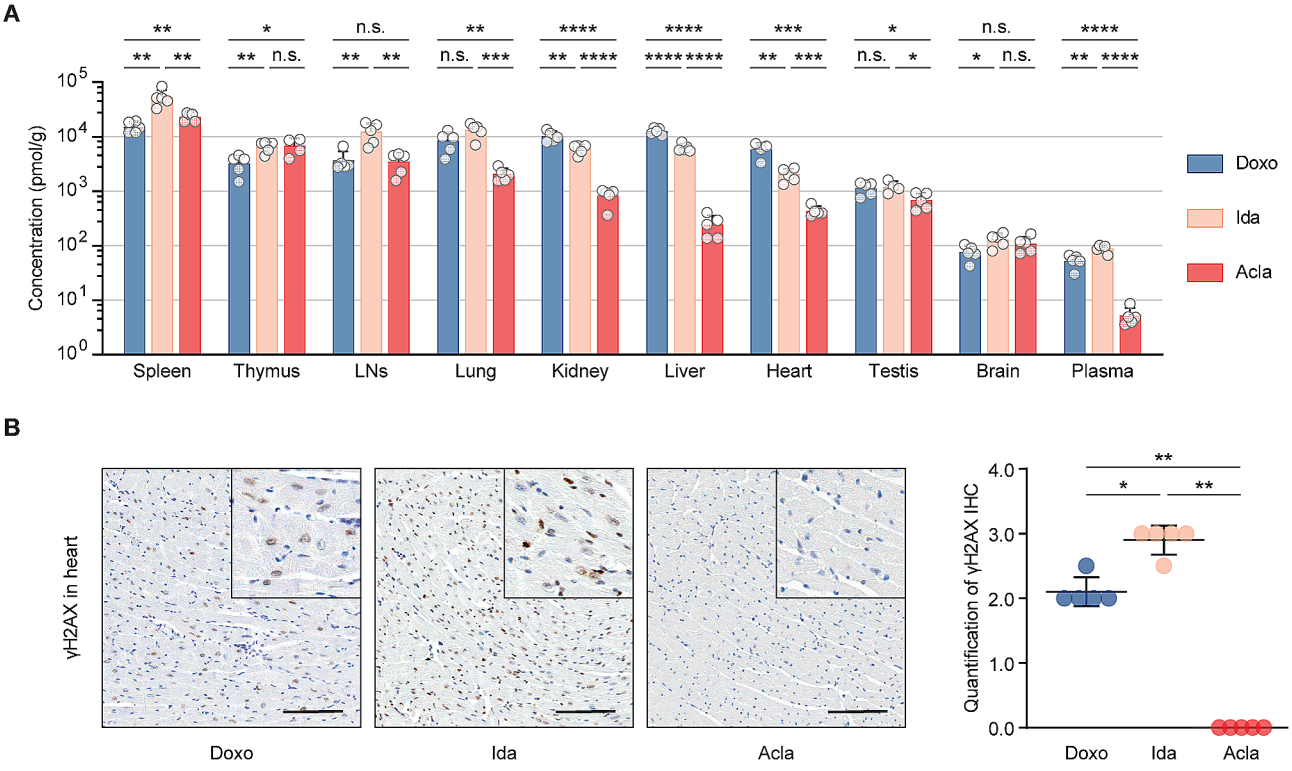

Fig. 3 Bio-distribution of clinically used anthracyclines in mice. (**A**) Drug bio-distribution was determined 4 h after i.v. injection of indicated drug at 5 mg/kg. Data are represented as mean ± SD from 5 mice per group. Student's *t*-test. (**B**) Representative microscopic images of γH2AX IHC staining of the hearts. Scale bars, 100 μm. Quantification is represented as mean ± SD, $n = 5$, Mann-Whitney test. *$P < 0.05$, **$P < 0.01$, ***$P < 0.001$, and ****$P < 0.0001$; n.s., not significant

minimal cross-resistance and distinct epigenomic specificities compared to other anthracyclines, Acla may act as an independent therapeutic agent in salvage relapsed/refractory AML (r/rAML) patients who have reached the maximum cumulative dose of cardiotoxic anthracyclines. However, systematic studies examining this aspect are lacking.

A combination therapy of cytarabine, aclarubicin and G-CSF (CAG) significantly improves the survival of r/rAML patients

r/rAML poses a significantly challenge in hematology, with a 5-year overall survival (OS) of only 10% [46]. The prognosis of elderly or unfit r/rAML patients is even more disappointing [47]. Unfortunately, no specific salvage regimen has emerged as a standard treatment for r/rAML [47]. The CAG regimen, containing low-dose cytarabine, Acla and G-CSF, has been widely used in China and Japan for treating AML [48, 49]. It is well tolerated by relapsed/refractory and elderly AML patients with lower toxicity than conventional chemotherapies [48–50]. To compare the efficacy of CAG to other salvage chemotherapies in r/rAML, we conducted a single-center retrospective study at Ruijin hospital (Shanghai, China).

A total of 186 r/rAML patients, treated between July 2012 and July 2022, were enrolled in the study. In this cohort, fit patients with *de novo* AML typically received Ida in combination with cytarabine (IA) for first-line therapy, as Ida is more effective than Doxo or Daun for AML induction therapy [51, 52]. However, all three anthracyclines are known to be cardiotoxic [53]. Among patients who developed refractory or relapse after primary IA treatment, 66 received CAG regimen (2^{nd}-line CAG group), 67 received other chemotherapy regimens (including IA, DA, FLAG, CLAAG and CHA regimens, named collectively as 2^{nd}-line others group), and 34 received emerging target therapy regimen venetoclax plus azacitidine (2^{nd}-line VA group) (Fig. 5A). Notably, at Ruijin hospital, CAG is also applied to unfit *de novo* AML patients who are ineligible for conventional intensive chemotherapies. Therefore, 19 such patients treated with CAG for both *de novo* and r/r diseases were included to illustrate the lack of cardiotoxicity of Acla and its compatibility with extended treatment (1^{st}&2^{nd}-line CAG group) (Fig. 5A). The demographic and clinical characteristics of all patients at r/rAML diagnosis are summarized in Table S1. There was no significant difference between 2^{nd}-line CAG group and any other group with respect to age, sex, French-American-British type, cytogenetic risk,

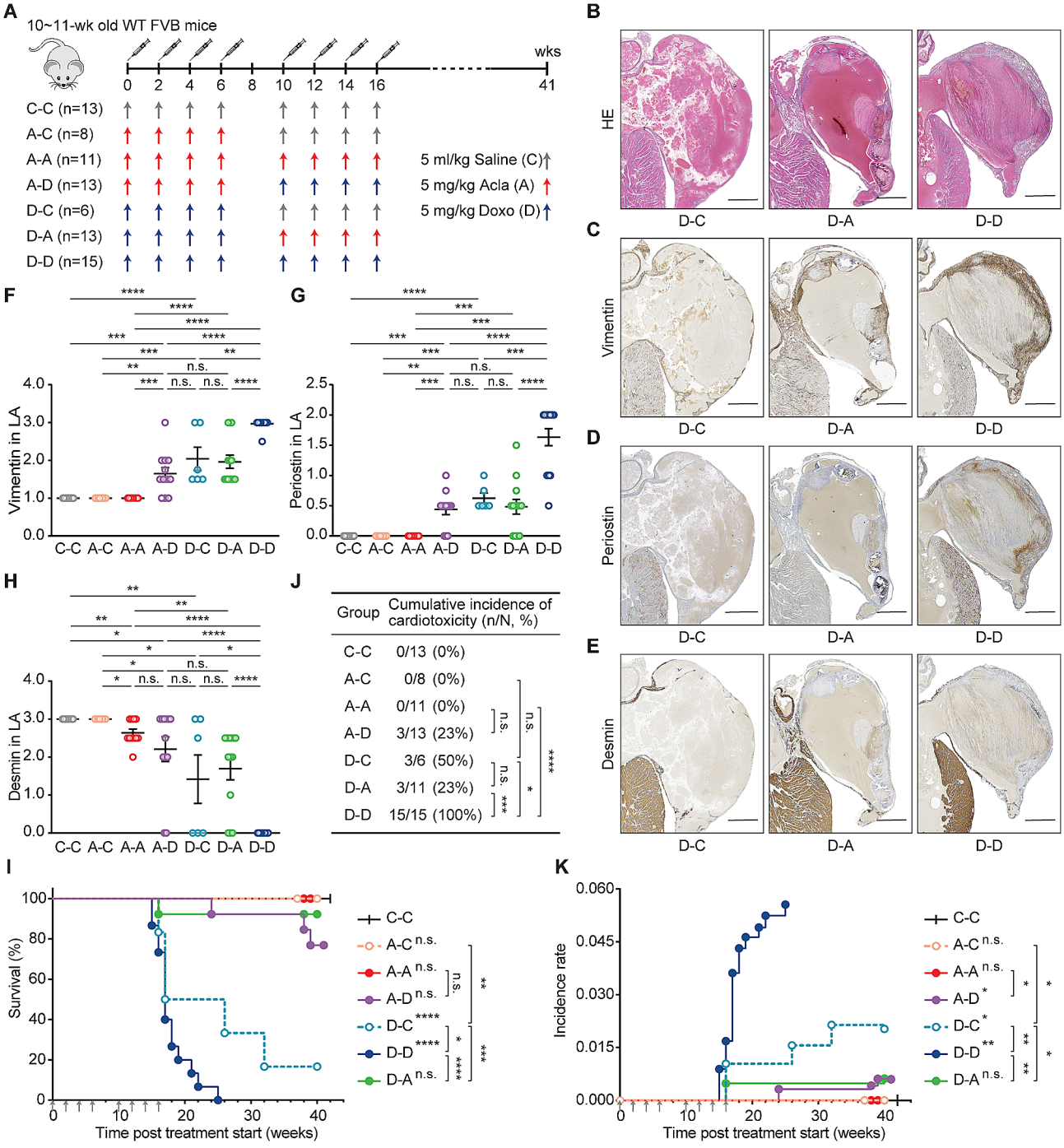

Fig. 4 Acla is safe and well tolerated following Doxo treatment. (**A**) Wild-type FVB mice were i.v. injected with Doxo (**D**), Acla (**A**), or saline (**C**) as indicated. (**B-E**) Representative microscopic images of the left atrium (LA) of heart. Lesions caused by Doxo treatment represent as impairment of the wall, thrombosis, inflammation, fibrosis/calcification, and disappearing of the lumen of atrium (filled by a large thrombus). Scale bars, 500 μm. (**F-H**) Quantification of the indicated IHC staining in LA. Data are mean ± SEM, Mann-Whitney test. (**I**) Animal survival is plotted in Kaplan-Meier curves. Log-rank test. (**J**) Cumulative incidence of cardiotoxicity. Fisher's exact test. (**K**) Incidence rate of cardiotoxicity. Two-way ANOVA with repeated measures, two-sided. *$P < 0.05$, **$P < 0.01$, ***$P < 0.001$, and ****$P < 0.0001$; n.s., not significant

A

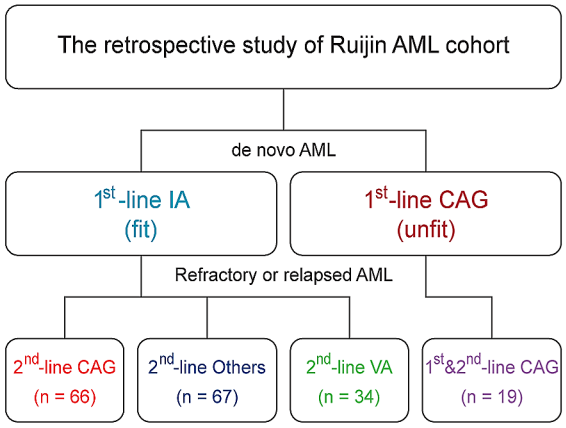

B

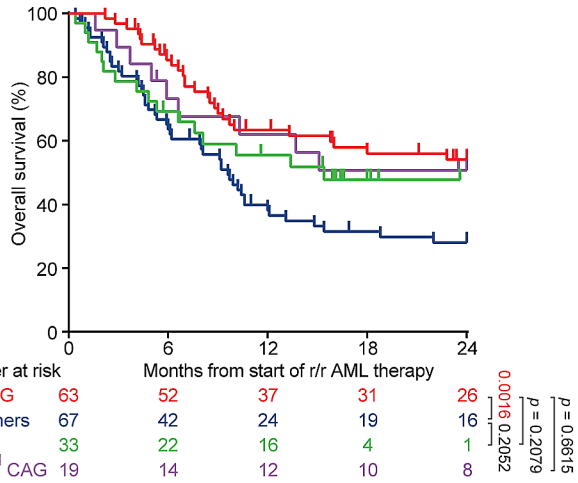

C

OS of r/rAML at 2 years	2nd-line CAG		2nd-line Others		2nd-line VA		1st&2nd-line CAG	
Overall		p value#		p value*		p value*		p value*
Survival	36/63 (57%)		21/67 (31%)	0.0045†	17/33 (52%)	0.6681†	10/19 (53%)	0.7952†
Median time (month)	NA		9.6	0.0016‡	15.4	0.2079‡	NA	0.6615‡
Hazard Ratio (95% CI)			2.109 (1.327 – 3.353)§		1.535 (0.7880 – 2.988)§		1.193 (0.5414 – 2.629)§	
Favourable and intermediate cytogenetics								
Survival	29/48 (60%)		17/58 (29%)	0.0017†	15/27 (56%)	0.8078†	7/14 (50%)	0.5475†
Median time (month)	NA		9.2	0.0004‡	NA	0.2901‡	15.1	0.4251‡
Hazard Ratio (95% CI)			2.538 (1.522 – 4.232)§		1.521 (0.6995 – 3.306)§		1.474 (0.5683 – 3.822)§	
Unfavourable cytogenetics								
Survival	4/11 (36%)	0.1873†	3/7 (43%)	>0.9999†	1/5 (20%)	>0.9999†	1/3 (33%)	>0.9999†
Median time (month)	9.3	0.0698‡	10.2	0.7269‡	4.8	0.4112‡	5	0.6809‡
Hazard Ratio (95% CI)	2.758 (0.9213 – 8.255)§		0.8071 (0.2424 – 2.687)§		1.769 (0.4538 – 6.894)§		1.441 (0.2525 – 8.225)§	

D

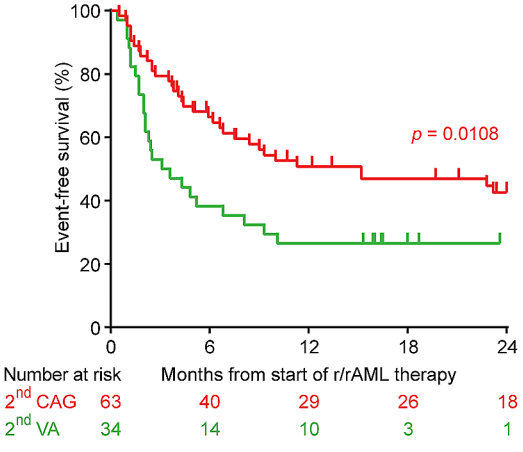

E

EFS of r/rAML at 2 years	2nd-line CAG		2nd-line VA	
Overall		p value#		p value*
Survival	29/63 (46%)		9/34 (26%)	0.0813†
Median time (month)	15.2		3.35	0.0108‡
Hazard Ratio (95% CI)			2.121 (1.190 – 3.782)§	
Favourable and intermediate cytogenetics				
Survival	23/48 (48%)		8/27 (30%)	0.1478†
Median time (month)	22.8		3.6	0.0166‡
Hazard Ratio (95% CI)			2.273 (1.161 – 4.449)§	
Unfavourable cytogenetics				
Survival	3/11 (27%)	0.3162†	1/5 (20%)	>0.9999†
Median time (month)	4.3	0.0684‡	1.7	0.7396‡
Hazard Ratio (95% CI)	2.543 (0.9318 – 6.942)§		1.212 (0.3493 – 4.207)§	

Fig. 5 CAG is effective in treating r/rAML patients. (**A**) The therapy overview of Ruijin AML cohort. CAG: cytarabin, aclarubicin, G-CSF; IA: idarubicin, cytarabine; VA: venetoclax, azacitidine; Others: chemotherapy regimens other than CAG. (**B**) Overall survival of the r/rAML patients from the start of r/rAML induction treatment to the date of death. Log-rank test. (**C**) The statistical analysis of OS of r/rAML patients at 2 years. Data are n/N (%), * compared with 2nd-line CAG group, † Fisher's exact test, ‡ Log-rank test, § Mantel-Haenszel test, # compared with 2nd-line CAG patients with favorable and intermediate cytogenetics. (**D**) Event-free survival of the r/rAML patients from the start of r/rAML induction treatment to the date of relapse/refractory/death. (**E**) The statistical analysis of EFS of r/rAML patients at 2 years. Data are n/N (%), * compared with 2nd-line CAG group, † Fisher's exact test, ‡ Log-rank test, § Mantel-Haenszel test, # compared with 2nd-line CAG patients with favorable and intermediate cytogenetics

or frequent oncogenic mutations. Slightly more patients in the 2nd-line others group were diagnosed with favorable integrated risk than in the other arms of the study.

The overall complete remission (CR) rate was 74% for the 2nd-line CAG group, significantly higher than that of the 2nd-line others (37%) and the 2nd-line VA group (35%) (Table 1). Patients with favorable and intermediate cytogenetics or integrated risk responded better to CAG, although these factors were not prognostic in the other groups (Table 1). As age being a poor prognostic factor for AML [47], in patients aged≥60-year-old, 2nd-line CAG also outperformed other treatment regimens (Table S2). No CR and major prognostic mutation associations were detected in any treatment group due to the small cohort size (Table S2). Despite slightly less optimal outcomes for the 1st&2nd-line CAG group due to unfit conditions, this treatment protocol remained non-inferior to the 2nd-line others and the 2nd-line VA group (Table 1; Table S2), suggesting the continued effectiveness and well tolerability of CAG in unfit r/rAML patients, even after prior CAG treatments.

Given to the favorable tolerability of both CAG and VA therapy, some patients continued with these regimens for consolidation therapy and long-term maintenance, with some patients receiving up to 11 cycles of CAG without any cardiac issues, a far more cumulative dose than other anthracyclines (Fig. S5A). This extended treatment strategy was not an option for other anthracyclines due to accumulated cardiotoxicity and resistance. The superior CR rates and/or sustainable treatment schedules of CAG and VA translated into a more than 20% better OS compared to 2nd-line others group (Fig. 5B, C; Fig. S5B, C). However, event-free survival analysis indicated a more durable response with 2nd-line CAG compared to 2nd-line VA (Fig. 5D, E), possibly due to the development of acquired resistance to VA [54]. Of note, the 1st&2nd-line CAG patients assign to this low toxic CAG regimen because of unfit conditions, achieved comparable OS as the 2nd-line CAG group (Fig. 5B, C; Fig. S5D, E). Taken together, these results reveal the potential of CAG regimen as a superior, low-toxicity chemotherapy for r/rAML, including the unfit cases.

Discussion

Anthracyclines like Doxo, Daun and Ida have been cornerstones of oncology treatment for over 50 years despite their devastating side effects. Contrary to the assumption of uniformity in molecular mechanisms across anthracycline analogs, our comprehensive analyses reveal substantial differences in mode of action, epigenomic selectivity, clinical performance, and pharmacological properties. In the course of our evaluation, we noted that Acla stands out for its potent anti-neoplastic effect, minimal cardiotoxicity and preferential distribution in lymphoid organs. The latter may explain the effectiveness of Acla in treating AML other than solid tumors. Attributing to its high therapeutic index for AML, we demonstrate that Acla can be safely used in second-line therapy following the treatment of cardiotoxic anthracyclines, leading to a 23% higher 5-year OS for r/rAML patients compared to other intensive chemotherapies.

DNA damage induced by TopoII poisoning has always been considered as the primary cytotoxic mechanism of anthracyclines [1]. However, this dogma is challenged by Acla and other anthracycline variants which predominantly elicit chromatin damage through histone eviction and TopoIIα redistribution [5, 55, 56]. TopoIIα plays roles in all areas of chromosome structure, including nucleosome turnover, chromosome condensation and segregation [57–59]. Moreover, it is exclusively expressed in proliferating compartments and is correlated with aggressive or rapidly proliferating cancers [60]. Deregulation of TopoIIα leads to cell death independent of its catalytic activity [61, 62]. Therefore, without poisoning TopoII for DNA damage, depleting and redistributing TopoIIα are cytotoxic, as observed with Acla, underscoring the significance of chromatin damage against cancer. Of note, the loss of TopoIIβ does not impede cell

Table 1 Treatment outcomes of r/rAML patients

Clinical outcome	2nd-line CAG		2nd-line Others			2nd-line VA			1st&2nd-line CAG		
Complete remission	(*n* = 65)		(*n* = 51)		*P* value	(*n* = 31)		*P* value	(*n* = 17)		*P* value
Overall	48/65	(74%)	19/51	(37%)	**0.0001†**	11/31	(35%)	**0.0006†**	10/17	(59%)	0.2433†
Complete remission		**0.0279‡**			> 0.9999‡			> 0.9999‡			0.5500‡
Favorable and intermediate cytogenetics	40/50	(80%)	17/46	(37%)	**< 0.0001†**	8/23	(35%)	**0.0004†**	8/13	(62%)	0.2704†
Unfavorable cytogenetics	5/11	(45%)	2/5	(40%)	> 0.9999†	2/5	(40%)	> 0.9999†	1/3	(33%)	> 0.9999†
Unknown cytogenetics	3/4	(75%)	0/0	(NA)	> 0.9999†	1/2	(50%)	> 0.9999†	1/1	(100%)	> 0.9999†
Complete remission		**0.0087‡**			> 0.9999‡			0.2553‡			> 0.9999‡
Favorable and intermediate integrated risk	34/40	(85%)	12/32	(38%)	**< 0.0001†**	5/19	(26%)	**< 0.0001†**	6/10	(60%)	0.0966†
Unfavorable integrated risk	9/18	(50%)	6/16	(38%)	0.7055†	6/12	(50%)	> 0.9999†	3/5	(60%)	> 0.9999†
Unknown integrated risk	5/7	(71%)	1/3	(33%)	0.5000†	0/0	(NA)	> 0.9999†	1/2	(50%)	> 0.9999†

CAG: cytarabin, aclarubicin, G-CSF; IA: idarubicin, cytarabine; VA: venetoclax, azacitidine; Others: chemotherapies other than CAG, including IA, DA, FLAG, CLAAG and CHA regimens. Data are n/N (%). † Fisher's exact test between the indicated group and 2nd-line CAG group. ‡ Fisher's exact test within group

proliferation [63] and its expression does not influence the treatment outcome of anthracycline-based therapy in AML patients. Yet, it plays multifaceted role in transcription regulation [64] and contributes to therapy-related malignancies [65]. Hence, further exploration is warranted to delineate the effects of individual anthracyclines on TopoIIβ.

While in vitro and preclinical models allow for controlled investigations of single agent, they may not fully reflect the complexities of clinical scenarios. Single-center retrospective analyses also have inherent limitations, such as relative low sample size and confounding variables. Our dataset included the information on many features such as age, sex and mutations, revealing no discernible bias in any of the treatment arms. This allowed us to compare the treatment results between the 2nd-line CAG and other groups. The relative small size of 1st&2nd-line CAG group and shorter follow-up of 2nd-VA group may impact the statistical power. Notably, the focus of the 1st&2nd-line CAG group centers on its low toxicity and low acquired resistance, while venetoclax was introduced into clinic very recently.

While Acla was first introduced into clinic 40 years ago (it was available in Europe until 2004 and was never registered in the U.S.), the unique effectiveness of Acla in r/rAML has been overlooked. Besides the improvement in OS of r/rAML patients by CAG therapy, the preliminary results from our research group also suggest the feasibility and tolerability of CAG-VA combination (unpublished observations) warranting further investigation into its efficacy. By repurposing old drugs like Acla, an estimated 10,000 r/rAML patients annually in the U.S. and Europe [66] could survive from this off-patent and low cost drug. The impact on pediatric oncology will be even more profound, as 50% of childhood cancer patients receive high-dose anthracyclines and go on to have a 5- to 15-fold increased risk for heart failure compared to the general population [13]. Introducing Acla could significantly mitigate this risk [5, 56]. Considering old drugs in new ways may therefore substantially – and expeditiously – improve the survival and quality of life of many cancer patients, as exemplified here. Expanding on these findings, a multicenter Phase III prospective study is scheduled to commence later this year in China and the Netherlands, aiming to incorporate Acla into the treatment of r/rAML patients.

Abbreviations

Acla	Aclarubicin
AML	Acute myeloid leukemia
Amr	Amrubicin
Ara-C	Cytarabine
ATAC-seq	Assay for Transposase-Accessible Chromatin using sequencing
ATRA	Retinoic acid
CAG	Cytarabine, Acla and G-CSF regimen
CFGE	Constant-field gel electrophoresis
CHA	Cladribine, homoharringtonine and Ara-C regimen
ChIP-seq	Chromatin immunoprecipitation followed by sequencing
CLAAG	Cladribine, Ara-C, ATRA and G-CSF regimen
CR	Complete remission
DA	Decitabine and Ara-C regimen
Daun	Daunorubicin
DHS	DNase I hypersensitive regions
Doxo	Doxorubicin
Epi	Epirubicin
FCS	Fetal calf serum
FLAG	Fludarabine, Ara-C and G-CSF regimen
FLT3-ITD	FLT3 internal tandem duplication
G-CSF	Granulocyte colony stimulating factor
GEO	Gene expression omnibus
IA	Ida and cytarabine regimen
Ida	Idarubicin
IMDM	Iscove's modified dulbecco's medium
IR	Incidence rate
i.v.	Intravenous(ly)
OS	Overall survival
PCA	Principal component analysis
γH2AX	phosphorylation of H2AX at Ser139
r/rAML	relapsed/refractory AML
s.c.	Subcutaneous(ly)
SDS	Sodium dodecyl sulfate
TopoII	Topoisomerase II
VA	Venetoclax and azacitidine regimen

Supplementary Information

The online version contains supplementary material available at https://doi.org/10.1186/s12943-024-02034-7.

Supplementary Material 1

Supplementary Material 2

Acknowledgements

The authors thank the people from the Preclinical Intervention Unit of the Mouse Clinic for Cancer and Ageing (MCCA) at NKI for their technical support performing the animal experiments and the staff from the Experimental Animal Pathology facility at NKI for their service on histochemistry and immunochemistry staining; Prof. J.P. Vandenbroucke and M. Schaapveld for help with the epidemiological assessment of clinical data; J. Sarthy, H. Ploegh and I. Berlin for comments and critical reading of the manuscript.
This manuscript is in memory of Koen Krabbenbos, a courageous young boy from the Netherlands. He was an AML patient who would have liked to participate in this research. Unfortunately Koen was not able to do so. He passed away at the age of 12.

Author contributions

X.Q., S.Y.v.d.Z. and J.N. designed experiments. X.Q. and S.Y.v.d.Z. performed experiments. O.v.T., F.L.H., and M.A.v.G. contributed to experiments. Y.Z. and X.L. collected the r/rAML data. X.Q., X.L., J.L. and J.N. analyzed the clinical data. M.T. and B.P. performed and analyzed ChIP-seq and ATAC-seq experiments. L.J., Y.L. and B.P. made stable cell lines. J.S. performed pathological analyses. C.L.Z. contributed to the result interpretation. X.Q., S.Y.v.d.Z. and J.N. wrote the manuscript, with the input of all authors. All authors read and approved the final manuscript.

Funding

This work was supported by grants from the European Research Council (ERC) (advanced grant ERCOPE 694307) (J.N.), Dutch Cancer Society (KWF 11356) (J.N.), Institute for Chemical Immunology from NWO Gravitation (NWO 024.002.009) (J.N.), Spinoza award funded by the Ministry of Education, Culture and Science of the Netherlands (NWO 00897590) (J.N.), RIKI foundation (C.L.Z.).

Data availability

The sequencing data supporting the findings of this study are available at the Gene Expression Omnibus (GEO) under accession numbers GSE240443 (https://www.ncbi.nlm.nih.gov/geo/query/acc.cgi?acc=GSE240443). Source data are provided with this paper. Clinical data are available from the

corresponding authors upon reasonable request and with permission of Ruijin hospital.

Declarations

Ethics approval and consent to participate
All mouse experiments were approved by the Animal Ethics Committee of the NKI and were performed according to institutional and national guidelines. The retrospective clinical study was approved by the ethics committee of Ruijin Hospital, and all patients provided written informed consent.

Competing interests
J.N. is a shareholder in NIHM that aims to produce Acla for clinical use. The authors do not declare any other competing interests.

Author details
[1]Division of Tumor Biology and Immunology, The Netherlands Cancer Institute, Amsterdam, The Netherlands
[2]Department of Head and Neck Oncology and Surgery, The Netherlands Cancer Institute, Amsterdam, The Netherlands
[3]Department of Cell and Chemical Biology, ONCODE Institute, Leiden University Medical Center, Leiden, The Netherlands
[4]Shanghai Institute of Hematology, State Key Laboratory of Medical Genomics, National Research Center for Translational Medicine, Ruijin Hospital Affiliated to Shanghai Jiao Tong University School of Medicine, Shanghai, China
[5]Division of Pharmacology, The Netherlands Cancer Institute, Amsterdam, The Netherlands
[6]Division of Experimental Animal Pathology, The Netherlands Cancer Institute, Amsterdam, The Netherlands
[7]Wuxi Branch of Ruijin Hospital, Ruijin Hospital, Shanghai Jiao Tong University School of Medicine, Shanghai 200025, China

Received: 22 November 2023 / Accepted: 28 May 2024
Published online: 04 June 2024

References

1. Tewey KM, Rowe TC, Yang L, Halligan BD, Liu LF. Adriamycin-induced DNA damage mediated by mammalian DNA topoisomerase II. Science. 1984;226(4673):466–8.
2. Pang B, Qiao X, Janssen L, Velds A, Groothuis T, Kerkhoven R, et al. Drug-induced histone eviction from open chromatin contributes to the chemotherapeutic effects of doxorubicin. Nat Commun. 2013;4:1908.
3. Pang B, de Jong J, Qiao X, Wessels LF, Neefjes J. Chemical profiling of the genome with anti-cancer drugs defines target specificities. Nat Chem Biol. 2015;11(7):472–80.
4. Yang F, Kemp CJ, Henikoff S. Doxorubicin enhances nucleosome turnover around promoters. Curr Biol. 2013;23(9):782–7.
5. Qiao X, van der Zanden SY, Wander DPA, Borras DM, Song JY, Li X, et al. Uncoupling DNA damage from chromatin damage to detoxify doxorubicin. Proc Natl Acad Sci USA. 2020;117(26):15182–92.
6. Girling DJ. Comparison of oral etoposide and standard intravenous multidrug chemotherapy for small-cell lung cancer: a stopped multicentre randomised trial. Med Res Council Lung Cancer Working Party Lancet. 1996;348(9027):563–6.
7. Hong WK, Nicaise C, Lawson R, Maroun JA, Comis R, Speer J, et al. Etoposide combined with cyclophosphamide plus vincristine compared with doxorubicin plus cyclophosphamide plus vincristine and with high-dose cyclophosphamide plus vincristine in the treatment of small-cell carcinoma of the lung: a randomized trial of the bristol lung cancer study group. J Clin Oncol. 1989;7(4):450–6.
8. Jin J, Wang JX, Chen FF, Wu DP, Hu J, Zhou JF, et al. Homoharringtonine-based induction regimens for patients with de-novo acute myeloid leukaemia: a multicentre, open-label, randomised, controlled phase 3 trial. Lancet Oncol. 2013;14(7):599–608.
9. Lotrionte M, Biondi-Zoccai G, Abbate A, Lanzetta G, D'Ascenzo F, Malavasi V, et al. Review and meta-analysis of incidence and clinical predictors of anthracycline cardiotoxicity. Am J Cardiol. 2013;112(12):1980–4.
10. Larsen CM, Garcia Arango M, Dasari H, Arciniegas Calle M, Adjei E, Rico Mesa J, et al. Association of anthracycline with heart failure in patients treated for breast cancer or lymphoma, 1985–2010. JAMA Netw Open. 2023;6(2):e2254669.
11. Volkova M, Russell R. 3rd. Anthracycline cardiotoxicity: prevalence, pathogenesis and treatment. Curr Cardiol Rev. 2011;7(4):214–20.
12. Sekeres MA, Guyatt G, Abel G, Alibhai S, Altman JK, Buckstein R, et al. American society of hematology 2020 guidelines for treating newly diagnosed acute myeloid leukemia in older adults. Blood Adv. 2020;4(15):3528–49.
13. Armenian S, Bhatia S. Predicting and preventing anthracycline-related cardiotoxicity. Am Soc Clin Oncol Educ Book. 2018;38:3–12.
14. Li Y, Tan M, Sun S, Stea E, Pang B. Targeted CRISPR activation and knockout screenings identify novel doxorubicin transporters. Cell Oncol (Dordr). 2023.
15. Wlodek D, Banath J, Olive PL. Comparison between pulsed-field and constant-field gel electrophoresis for measurement of DNA double-strand breaks in irradiated Chinese hamster ovary cells. Int J Radiat Biol. 1991;60(5):779–90.
16. van der Kant R, Fish A, Janssen L, Janssen H, Krom S, Ho N, et al. Late endosomal transport and tethering are coupled processes controlled by RILP and the cholesterol sensor ORP1L. J Cell Sci. 2013;126(Pt 15):3462–74.
17. Schmidt D, Wilson MD, Spyrou C, Brown GD, Hadfield J, Odom DT. ChIP-seq: using high-throughput sequencing to discover protein-DNA interactions. Methods. 2009;48(3):240–8.
18. Langmead B, Salzberg SL. Fast gapped-read alignment with Bowtie 2. Nat Methods. 2012;9(4):357–9.
19. Kharchenko PV, Tolstorukov MY, Park PJ. Design and analysis of ChIP-seq experiments for DNA-binding proteins. Nat Biotechnol. 2008;26(12):1351–9.
20. Amemiya HM, Kundaje A, Boyle AP. The ENCODE blacklist: identification of problematic regions of the genome. Sci Rep. 2019;9(1):9354.
21. Roadmap Epigenomics C, Kundaje A, Meuleman W, Ernst J, Bilenky M, Yen A, et al. Integrative analysis of 111 reference human epigenomes. Nature. 2015;518(7539):317–30.
22. Ross-Innes CS, Stark R, Teschendorff AE, Holmes KA, Ali HR, Dunning MJ, et al. Differential oestrogen receptor binding is associated with clinical outcome in breast cancer. Nature. 2012;481(7381):389–93.
23. Buenrostro JD, Giresi PG, Zaba LC, Chang HY, Greenleaf WJ. Transposition of native chromatin for fast and sensitive epigenomic profiling of open chromatin, DNA-binding proteins and nucleosome position. Nat Methods. 2013;10(12):1213–8.
24. Corces MR, Trevino AE, Hamilton EG, Greenside PG, Sinnott-Armstrong NA, Vesuna S, et al. An improved ATAC-seq protocol reduces background and enables interrogation of frozen tissues. Nat Methods. 2017;14(10):959–62.
25. Zhang Y, Liu T, Meyer CA, Eeckhoute J, Johnson DS, Bernstein BE, et al. Model-based analysis of ChIP-Seq (MACS). Genome Biol. 2008;9(9):R137.
26. Slovak ML, Kopecky KJ, Cassileth PA, Harrington DH, Theil KS, Mohamed A, et al. Karyotypic analysis predicts outcome of preremission and postremission therapy in adult acute myeloid leukemia: a Southwest oncology group/Eastern cooperative oncology group study. Blood. 2000;96(13):4075–83.
27. Dohner H, Estey EH, Amadori S, Appelbaum FR, Buchner T, Burnett AK, et al. Diagnosis and management of acute myeloid leukemia in adults: recommendations from an international expert panel, on behalf of the European LeukemiaNet. Blood. 2010;115(3):453–74.
28. Greene RF, Collins JM, Jenkins JF, Speyer JL, Myers CE. Plasma pharmacokinetics of adriamycin and adriamycinol: implications for the design of in vitro experiments and treatment protocols. Cancer Res. 1983;43(7):3417–21.
29. Kuo LJ, Yang LX. Gamma-H2AX - a novel biomarker for DNA double-strand breaks. vivo. 2008;22(3):305–9.
30. Cox J, Weinman S. Mechanisms of doxorubicin resistance in hepatocellular carcinoma. Hepat Oncol. 2016;3(1):57–9.
31. Chen YL, Yang TY, Chen KC, Wu CL, Hsu SL, Hsueh CM. Hypoxia can impair doxorubicin resistance of non-small cell lung cancer cells by inhibiting MRP1 and P-gp expression and boosting the chemosensitizing effects of MRP1 and P-gp blockers. Cell Oncol (Dordr). 2016;39(5):411–33.
32. Wang AH, Ughetto G, Quigley GJ, Rich A. Interactions between an anthracycline antibiotic and DNA: molecular structure of daunomycin complexed to d(CpGpTpApCpG) at 1.2-A resolution. Biochemistry. 1987;26(4):1152–63.
33. Gerstein MB, Kundaje A, Hariharan M, Landt SG, Yan KK, Cheng C, et al. Architecture of the human regulatory network derived from ENCODE data. Nature. 2012;489(7414):91–100.
34. Imre L, Simandi Z, Horvath A, Fenyofalvi G, Nanasi P, Niaki EF, et al. Nucleosome stability measured in situ by automated quantitative imaging. Sci Rep. 2017;7(1):12734.

35. Barski A, Cuddapah S, Cui K, Roh TY, Schones DE, Wang Z, et al. High-resolution profiling of histone methylations in the human genome. Cell. 2007;129(4):823–37.
36. Alvarez F, Munoz F, Schilcher P, Imhof A, Almouzni G, Loyola A. Sequential establishment of marks on soluble histones H3 and H4. J Biol Chem. 2011;286(20):17714–21.
37. Rea S, Eisenhaber F, O'Carroll D, Strahl BD, Sun ZW, Schmid M, et al. Regulation of chromatin structure by site-specific histone H3 methyltransferases. Nature. 2000;406(6796):593–9.
38. Kerpel-Fronius S, Gyergyay F, Hindy I, Decker A, Sawinsky I, Faller K, et al. Phase I-II trial of aclacinomycin A given in a four-consecutive-day schedule to patients with solid tumours. A South-East European Oncology Group (SEEOG) Study. Oncology. 1987;44(3):159–63.
39. Martino S, Decker DA, Hynes HE, Kresge CL. Phase II evaluation of aclacinomycin-A in advanced ovarian carcinoma. Investig New Drugs. 1987;5(4):373–4.
40. Johnson SA, Richardson DS. Anthracyclines in haematology: pharmacokinetics and clinical studies. Blood Rev. 1998;12(1):52–71.
41. Ando S, Nakamura T, Kagawa D, Ueda T, Nishimura T, Kubo A, et al. Pharmacokinetics of aclarubicin and its metabolites in humans and their disposition in blood cells. Cancer Treat Rep. 1986;70(7):835–41.
42. Fujihira S, Yamamoto T, Matsumoto M, Yoshizawa K, Oishi Y, Fujii T, et al. The high incidence of atrial thrombosis in mice given doxorubicin. Toxicol Pathol. 1993;21(4):362–8.
43. Lencova-Popelova O, Jirkovsky E, Mazurova Y, Lenco J, Adamcova M, Simunek T, et al. Molecular remodeling of left and right ventricular myocardium in chronic anthracycline cardiotoxicity and post-treatment follow up. PLoS ONE. 2014;9(5):e96055.
44. Zhao S, Wu H, Xia W, Chen X, Zhu S, Zhang S, et al. Periostin expression is upregulated and associated with myocardial fibrosis in human failing hearts. J Cardiol. 2014;63(5):373–8.
45. Guo R, Hua Y, Ren J, Bornfeldt KE, Nair S. Cardiomyocyte-specific disruption of Cathepsin K protects against doxorubicin-induced cardiotoxicity. Cell Death Dis. 2018;9(6):692.
46. Ganzel C, Sun Z, Cripe LD, Fernandez HF, Douer D, Rowe JM, et al. Very poor long-term survival in past and more recent studies for relapsed AML patients: the ECOG-ACRIN experience. Am J Hematol. 2018;93(8):1074–81.
47. Dohner H, Estey E, Grimwade D, Amadori S, Appelbaum FR, Buchner T, et al. Diagnosis and management of AML in adults: 2017 ELN recommendations from an international expert panel. Blood. 2017;129(4):424–47.
48. Yamada K, Furusawa S, Saito K, Waga K, Koike T, Arimura H, et al. Concurrent use of granulocyte colony-stimulating factor with low-dose cytosine arabinoside and aclarubicin for previously treated acute myelogenous leukemia: a pilot study. Leukemia. 1995;9(1):10–4.
49. Wei G, Ni W, Chiao JW, Cai Z, Huang H, Liu D. A meta-analysis of CAG (cytarabine, aclarubicin, G-CSF) regimen for the treatment of 1029 patients with acute myeloid leukemia and myelodysplastic syndrome. J Hematol Oncol. 2011;4:46.
50. Jin J, Chen J, Suo S, Qian W, Meng H, Mai W, et al. Low-dose cytarabine, aclarubicin and granulocyte colony-stimulating factor priming regimen versus idarubicin plus cytarabine regimen as induction therapy for older patients with acute myeloid leukemia. Leuk Lymphoma. 2015;56(6):1691–7.
51. Owattanapanich W, Owattanapanich N, Kungwankiattichai S, Ungprasert P, Ruchutrakool T. Efficacy and toxicity of Idarubicin Versus high-dose daunorubicin for induction chemotherapy in adult Acute myeloid leukemia: a systematic review and Meta-analysis. Clin Lymphoma Myeloma Leuk. 2018;18(12):814–21. e3.
52. Wang H, Xiao X, Xiao Q, Lu Y, Wu Y. The efficacy and safety of daunorubicin versus idarubicin combined with cytarabine for induction therapy in acute myeloid leukemia: a meta-analysis of randomized clinical trials. Med (Baltim). 2020;99(24):e20094.
53. McGowan JV, Chung R, Maulik A, Piotrowska I, Walker JM, Yellon DM. Anthracycline Chemotherapy and Cardiotoxicity. Cardiovasc Drugs Ther. 2017;31(1):63–75.
54. DiNardo CD, Tiong IS, Quaglieri A, MacRaild S, Loghavi S, Brown FC, et al. Molecular patterns of response and treatment failure after frontline venetoclax combinations in older patients with AML. Blood. 2020;135(11):791–803.
55. Wander DPA, van der Zanden SY, Vriends MBL, van Veen BC, Vlaming JGC, Bruyning T, et al. Synthetic (N,N-Dimethyl)doxorubicin glycosyl diastereomers to dissect modes of action of Anthracycline Anticancer drugs. J Org Chem. 2021;86(8):5757–70.
56. Wooten M, Takushi B, Ahmad K, Henikoff S. Aclarubicin stimulates RNA polymerase II elongation at closely spaced divergent promoters. Sci Adv. 2023;9(24):eadg3257.
57. DiNardo S, Voelkel K, Sternglanz R. DNA topoisomerase II mutant of Saccharomyces cerevisiae: topoisomerase II is required for segregation of daughter molecules at the termination of DNA replication. Proc Natl Acad Sci USA. 1984;81(9):2616–20.
58. Uemura T, Yanagida M. Isolation of type I and II DNA topoisomerase mutants from fission yeast: single and double mutants show different phenotypes in cell growth and chromatin organization. EMBO J. 1984;3(8):1737–44.
59. Uemura T, Ohkura H, Adachi Y, Morino K, Shiozaki K, Yanagida M. DNA topoisomerase II is required for condensation and separation of mitotic chromosomes in S. Pombe. Cell. 1987;50(6):917–25.
60. Turley H, Comley M, Houlbrook S, Nozaki N, Kikuchi A, Hickson ID, et al. The distribution and expression of the two isoforms of DNA topoisomerase II in normal and neoplastic human tissues. Br J Cancer. 1997;75(9):1340–6.
61. Holm C, Goto T, Wang JC, Botstein D. DNA topoisomerase II is required at the time of mitosis in yeast. Cell. 1985;41(2):553–63.
62. McPherson JP, Goldenberg GJ. Induction of apoptosis by deregulated expression of DNA topoisomerase IIalpha. Cancer Res. 1998;58(20):4519–24.
63. Dereuddre S, Delaporte C, Jacquemin-Sablon A. Role of topoisomerase II beta in the resistance of 9-OH-ellipticine-resistant Chinese hamster fibroblasts to topoisomerase II inhibitors. Cancer Res. 1997;57(19):4301–8.
64. Madabhushi R. The roles of DNA topoisomerase IIbeta in transcription. Int J Mol Sci. 2018;19(7).
65. Azarova AM, Lyu YL, Lin CP, Tsai YC, Lau JY, Wang JC, et al. Roles of DNA topoisomerase II isozymes in chemotherapy and secondary malignancies. Proc Natl Acad Sci USA. 2007;104(26):11014–9.
66. Seattle, IfHMaEI, United States. Global Burden of Disease Study 2019 Results. Global Burden of Disease Collaborative Network. 2020:https://vizhub.healthdata.org/gbd-results/

Publisher's Note